AADE-15-NTCE-33

Real Time Monitoring of Piezoresistive Smart Cement to Verify Oil Well Cementing Operations Using Simulated Physical Model Tests

Cumaraswamy Vipulanandan, Praveen Ramanathan, Kausar Ali and Bahareh Basirat, CIGMAT-University of Houston

Abstract

With increased drilling depths for production of oil and gas there are greater challenges due to changes in the ground conditions with in situ pressure and temperature conditions. Recent case studies on oil well failures have clearly identified cementing and drilling mud contamination as some of the issues that resulted in various types of delays in the cementing operations. For a successful cementing operation, it is critical to monitor the drilling and cementing operation during the installation so that necessary remediation can be made to minimize the delays and losses of cement. At present there is no technology available to monitor cementing operations without using buried sensors within the cement sheath and also monitor the movement of the drilling mud and spacer fluid to determine the changes real time during the installation of the oil wells.

In this study, small oil well models were designed, built and used to demonstrate the concept of real time monitoring of the flow of smart drilling mud and smart cement and hardening of the cement sheath in place. Also a new method has been developed to monitor the electrical resistivity of the materials using the two probe method. Based on the test results it has been proven that resistivity dominates the behavior of drilling mud and smart cement. LCR meters (measures the inductance (L), capacitance (C) and resistance (R)) were used at 300 kHz frequency to measure the changes in resistance. Several laboratory scale model tests have been performed using instrumented casing with wires and thermo couples. When the drilling mud was in the model borehole the measured resistance was the highest based on the high resistivity of the drilling mud. Notable reduction in electrical resistance was observed with the flow of spacer fluid and cement. Change in the resistance of hardened cement has been continuously monitored up to about 100 days. The predicted and the measured electrical resistances of the hardening cement sheath outside the cemented casing agreed very well. Also the pressure testing showed the piezoresistive response of the hardened smart cement.

Introduction

As Deepwater exploration and production of oil and gas expands around the world, there are unique challenges in well construction beginning at the seafloor. Also preventing the loss of fluids to the formations and proper well cementing have become critical issues in well construction to ensure wellbore integrity because of varying downhole conditions (Labibzadeh et al. 2010; Eoff et al. 2009; Ravi et al. 2007; Gill et al. 2005; Fuller et al. 2002). Moreover the environmental friendliness of the mud and cements is a critical issue that is becoming increasingly important (Durand et al. 1995; Thaemlitz et al. 1999; Dom et al. 2007). Lack of mud and cement returns may compromise the casing support and excess cement returns cause problems with flow and control lines (Ravi et al. 2007; Gill et al. 2005; Fuller et al. 2002). Hence there is a need for minimizing fluid losses by proper placement and monitoring of the drilling mud and cementing operation in real time. Unexpected fluid losses could be addressed real-time by changing the compositions of the drilling mud and/or cement slurry if real-time monitoring becomes available.

Successful deepwater cementing requires minimum fluid loss with drilling mud and cement slurry unit weights compatible with the formation (Eoff et al. 2009; Griffith et al. 1997). There are number of challenges associated with installation of casings in deepwater. The challenges include low fracture gradients resulting from young unconsolidated sands and shallow drilling hazards such as shallow water flows or hydrate formations, bottom-hole temperature and pressure, rapidly varying geological formations, fluid loss and no real-time monitoring of the operations. Recent case studies in the Gulf of Mexico (GOM) have documented using specially formulated lightweight foamed cement slurry to avoid cement sheath damage caused by shallow-water flow.

Two separate studies performed on oil well blowouts in the U.S. coastal area, one done between the years of 1971 to 1991 and the other study was done during the period of 1992 to 2006, before the deepwater horizon blowout in the Gulf of Mexico in 2010. The two studies clearly identified cement failures as the major cause for blowouts [Izod et al. 2007].

Cementing failures increased significantly during the second period of study when 18 of the 39 blowouts were due to cementing problems [Izod et al. 2007]. Also the deep-water horizon blowout in the Gulf of Mexico in 2010, where there was eleven fatalities, was due to cementing issues [Carter et al. 2014]. With some of the reported failures and growing interest of environmental and economic concerns in the oil and gas industry, integrity of the cement sheath is of major importance. At present there is no technology available to monitor the cementing operation real time from the time of placement through the entire service life of the borehole. Also there is no reliable method to determine the length of the competent cement supporting the casing.

Drilling Muds

Drilling mud is used for cuttings removal, suspension of cuttings, release of cuttings at seafloor, minimizing formation damage, reducing filtration rate, cooling and the lubrication of the drill bit and drill string, buoyancy support of the drill string and corrosion prevention. Drilling mud consists of two phases namely the liquid phase (water or oil) which is the base and the solid phase which is the clay and additives.

In general, composition of drilling mud is selected based on the guidelines set by the American Petroleum Institute (API). The drilling mud systems are broadly characterized as water, oil and synthetic based muds.

Water-based muds (WBM)

The basic composition of water based muds is water, clay and additive chemicals. The most common of clay used is bentonite and is frequently referred to as 'gel' in the oilfield applications. Gel likely makes reference to the fact that while the fluid is being pumped, it can be very thin and free-flowing (like chocolate milk), though when pumping is stopped, the static fluid builds a "gel" structure that resists flow. When an adequate pumping force is applied to "break the gel", flow resumes and the fluid returns to its previously free-flowing state. Many other chemicals like potassium salts are added to a WBM system to achieve various effects, including: viscosity control, shale stability, enhance drilling rate of penetration, cooling and lubricating of equipment.

Oil Well Cements (OWC)

Oil well cementing is done to provide a protective seal to the casing, prevent lost circulation and blowout and to promote zonal isolation. The standards of API suggest the chemical requirements determined by ASTM procedures and physical requirements determined in accordance with procedures outlined in API RP 10B and ASTM. There are classes A through H cements which could be used for oil well cementing.

Cement slurry flow ability and stability are the major requirements of oil well cementing. Oil-well cements (OWCs) are usually made from Portland cement clinker or from blended hydraulic cements. OWCs are classified into grades based upon their $Ca_3Al_nO_p$ (Tricalcium Aluminate – C_3A) content: Ordinary (O), Moderate Sulphate Resistant (MSR), and High Sulphate Resistant (HSR). Each class is applicable for a certain range of well depth, temperature, pressure, and sulphate environments. OWCs usually have lower C_3A contents, are coarsely ground, and may contain friction-reducing additives and special retarders such as starch and/or sugars in addition to or in place of gypsum.

Cements such as class G and class H, considered to be two of the popular cements, are used in oil well cementing applications. These cements are produced by pulverizing clinker consisting essentially of calcium silicates ($Ca_nSi_mO_p$) with the addition of calcium sulphate ($CaSO_4$) (John, 1992). Class H cement is produced by a similar process, except that the clinker and gypsum are ground relatively coarser than for a Class G cement, to give a cement with a surface area generally in the range 220-300 m^2/kg (John, 1992). Cementing is an important operation at the time of oil well construction (Backe et al., 1997). When admixtures are added with cement, tensile and flexural properties will be modified. Also admixtures will have effect on the rheological, corrosion resistance, shrinkage, thermal conductivity, specific heat, electrical conductivity and absorbing (heat and energy) properties of oil well cement (Bao-guo, 2008). Oil well cement slurry is used several thousand feet below the ground level and hence determining cement setting time is always a challenge.

Objectives

The major objective was to demonstrate the monitoring of the installation of the oil wells using the smart oil based drilling mud, smart spacer fluid and smart cement. Also investigate the monitoring of the curing of the cement sheath outside the casing and the piezoresistive response of the smart cement to applied pressures.

The specific objectives were as follows:

(1) Monitor the changes in the electrical resistance outside the casing during drilling and cementing.
(2) Monitor and predict the changes in electrical resistance of the hardening cement sheath outside the casing.
(3) Verify the piezoresistive response of the cement sheath.

Theory and Concepts

It was very critical to identify the sensing properties for the cement and drilling mud that can be used to monitor the performance. After years of studies and based on the current study on oil well cements and drilling muds, electrical resistivity (ρ) was selected as the sensing property for both cements and drilling muds. This makes it unique since same monitoring system can be used to evaluate the performance of the cement and drilling muds. Hence two parameters (resistivity and change in resistivity) will be used to quantify the sensing properties as follows:

$$R = \rho (L/A) = \rho K \quad \text{.....(1)}$$

Where, R = electrical resistance, L = Linear distance between the electrical resistance measuring points, A=

effective cross sectional area, K = Calibration parameter is determined based on the resistance measurement method.

Normalized change in resistivity with the changing conditions can be represented as follows:

$\Delta\rho/\rho = \Delta R/R$ ..... (2)

In resistivity of the materials (ρ) to changes (composition, curing, stress, fluid loss and temperature) has been quantified. Typical properties such as composition, curing, fluid loss and temperature are related to the resistivity (ρ) (Eqn. (1)). The change in resistivity (Δρ) (Eqn. (2)) will support the monitoring of the changes in the material (cement and drilling mud/fluid) behavior.

Impedence Spectroscopy (IS) Model (Vipulanandan et al. 2013)

Equivalent Circuit

Identification of the most appropriate equivalent circuit to represent the electrical properties of a material is essential to further understand its properties. In this study, an equivalent circuit to represent the Smart Cement and Smart Drilling Mud was required for better characterization through the analyses of the IS data. There were many difficulties associated with choosing a correct equivalent circuit. It was necessary somehow to make a link between the different elements in the circuit and the different regions in the impedance data of the corresponding sample. Given the difficulties and uncertainties, approach is to use circuits which most appropriate from the expected behavior of the material under study.

In this study, different possible equivalent circuits were analyzed to find an appropriate equivalent circuit to represent the smart cement and drilling mud.

Case 1: General Bulk Material – Resistance and Capacitor

In the equivalent circuit for Case1, the contacts were connected in series, and both the contacts and the bulk material were represented using a capacitor and a resistor connected in parallel (Fig. 1).

In the equivalent circuit for Case 1, R_b and C_b are resistance and capacitance of the bulk material, respectively and R_c and C_c are resistance and capacitance of the contacts, respectively. Both contacts are represented with the same resistance (R_c) and capacitance (C_c) as they are identical. Total impedance of the equivalent circuit for Case 1 (Z_1) can be represented as follows:

$$Z_1(\sigma) = \frac{R_b(\sigma)}{1+\omega^2 R_b^2 C_b^2} + \frac{2R_c(\sigma)}{1+\omega^2 R_c^2 C_c^2} - j\left\{\frac{2\omega R_c^2 C_c(\sigma)}{1+\omega^2 R_c^2 C_c^2} + \frac{\omega R_b^2 C_b(\sigma)}{1+\omega^2 R_b^2 C_b^2}\right\}, \quad ..(3)$$

where ω is the angular frequency of the applied signal. When the frequency of the applied signal was very low, $\omega \rightarrow 0$, $Z_1 = R_b + 2R_c$, and when it is very high, $\omega \rightarrow \infty$, $Z_1 = 0$.

Case 2: Special Bulk Material - Resistance Only

In Case 2, as a special case of Case 1, the capacitance of the bulk material (C_b) was assumed to be negligible (Fig.2). The total impedance of the equivalent circuit for Case 2 (Z_2) is as follows:

$$Z_2(\sigma) = R_b(\sigma) + \frac{2R_c(\sigma)}{1+\omega^2 R_c^2 C_c^2} - j\frac{2\omega R_c^2 C_c(\sigma)}{1+\omega^2 R_c^2 C_c^2}. \quad \text{……..(4)}$$

When the frequency of the applied signal was very low, $\omega \rightarrow 0$, $Z_2 = R_b + 2R_c$, and when it is very high, $\omega \rightarrow \infty$, $Z_2 = R_b$ (Fig. 3).

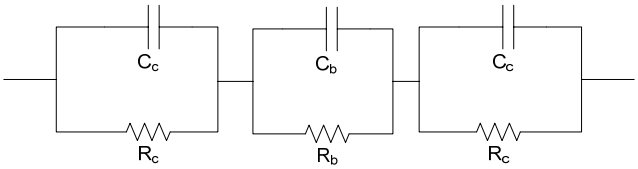

Figure 1. Equivalent circuit for Case1

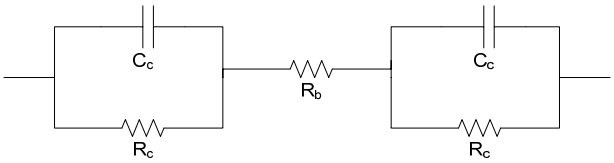

Figure 2. Equivalent circuit for Case 2

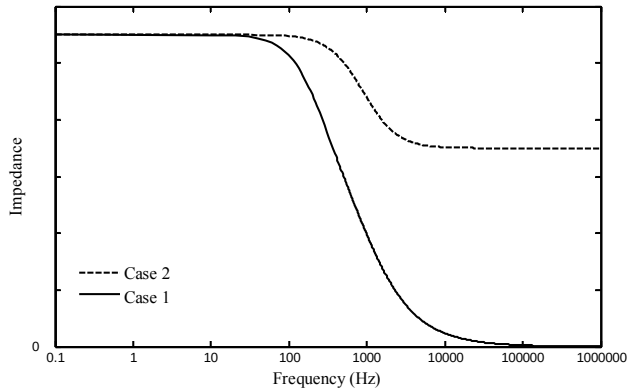

Figure 3. Comparison of typical responses of equivalent circuits for Case 1 and Case 2

Testing of smart cement, smart spacer fluid and smart drilling mud clearly indicated that Case 2 represented their behavior at a frequency of 300 kHz.

Materials and Methods

In this study, water based drilling mud and smart cement were used.

Water Based Mud

The electrical resistivity of the water that was used to prepare drilling fluid was 20 Ω.m.

Smart Cement

Oil well cement class H was used with a water-to-cement ratio 0.38. The cement was modified with an addition of 0.075% conductive filler by the total weight of the cement slurry. The initial resistivity of the cement slurry was 1.06 Ω.m. Typical piezoresistive response after one day of curing of the smart cement with water-to-cement ratio of 0.38 used in this study is shown in Fig 4.

Model

Laboratory models were designed and built at the University of Houston. The model was built to monitor the slurry level (drilling mud, spacer fluid and cement) during the installation and hardening of the cement. The observed resistance with time clearly indicated the level of slurry and to determine the depth at which the drilling fluid and cement was located. Several models were built separately and tested separately to demonstrate the real-time monitoring

The model was built using a flexi glass and metal pipe as shown in the Fig. 5 to simulate the formation and casing. The casing was instrumented with electrical wires to monitor the resistance change. The distance between two sensors was 4 to 6 inches and there were six levels of sensors as shown in the Fig. 5. Different combinations of the sensors were connected to a 300 Hz LCR device to measure resistance between those sensors. The horizontal electrical wire leads (sensors/monitors) are noted as a, b, c or d. The vertical wire leads are marked by 1 to 6. Figure 5 shows the different levels of liquid in the simulated well.

Results and Discussion

Monitoring the Drilling Mud (Water) Level

Resistance measured for different vertical levels of well is shown in Fig. 6. When there was no water in the well (at 0 level of water) the resistance was in the range of 450 to 650 kΩ which can be considered as the air resistance for the particular distance monitored at the relative humidity of the lab. When water level rose to level 1, all the vertical resistances dropped down to a range of 80 to 120 kΩ. This sudden change clearly showed that water reached level 1.

When water reached level 2, all vertical resistance combinations observed a small reduction in their values. But sensors c1-c2 (resistance in section-c and vertical line between level 1 and 2) observed drastic change in the resistance. It went down to about 1k Ω from about 95 k Ω. It happened because the earlier air resistance was replaced by water resistance when water fills the space between level 1 and 2 while the others levels experienced air resistance.

When water reached level 3, resistance between c1-c3 reduced drastically. The same pattern was observed for other sets of readings too, as shown in the Fig. 6. This consistent behavior showed that the level of the drilling fluid can be monitored effectively by measuring the resistance. The continuous reduction in the resistance was observed in the model with the rising water level. When the water level went upwards, air was replaced by water gradually. Water has relatively lesser resistance than air. Water and air can be considered here as connected in series. So the resulting resistance reduced with rising water level. And the drastic change was observed when the circuit was completed with water, without any air.

Figure 7 shows the changes in the resistance for horizontal level of sensing points. When water reached each horizontal level, the resistance dropped from several hundred kΩ to few ohms. This sudden change in the resistance indicated that the level of the water reached up to that particular height.

Figure 8 shows how the resistance changed with different levels of water for individual horizontal levels monitored. When the water level reached each level, resistance for that level reduced suddenly. For example, resistance between a3 and c3 (at horizontal level 3) reduced drastically when the water reached level 3.

Monitoring the Cement Slurry Level

The same procedure was used to demonstrate the smart cement slurry rise and the vertical resistances are reported in Figure 9. Similar pattern to water rise was observed which enabled the sensing method to detect the level of the cement slurry.

In contrast to 1000 Ω resistance of the drilling mud (water) the rage of resistance of cement slurry was in the range of 20 to 50 Ω for the time interval monitored. This observation showed that the material can be distinguished based on the resistance value while identifying the level of the slurry.

With time when the cement started to set, due to bleeding in the cement slurry free water accumulated above the cement. This effect was demonstrated by using the cement slurry with a water-to-cement ratio of 0.8. As shown in the Fig. 10, the resistance measurements clearly distinguished between free water and cement. At the earlier part of the experiments the water resistance was found to be in the range of 1000 Ω. But the free water resistance value was in the range of 30 to 40 Ω because of the mixed ions from the cement slurry. This observation showed that, using these resistance measurements, free water also can be detected.

Horizontal resistance measurements for cement slurry are reported in Fig. 11, which showed similar pattern to the drilling mud (water). This observation again confirmed that the cement slurry level can be detected using resistance measurement. Figure 12, shows the resistance variation with rising smart cement slurry level of each level of sensors which is again similar to that of drilling mud.

Curing of Cement Sheath

Resistivity of the smart cement

The Resistivity of the cement slurry with curing time of up to 100 days was determined using the smart cement slurry samples (2 inches diameter and 4 inches height cylindrical mold) that was used for the small model study. The resistivity increased with curing time under the curing of room temperature and humidity (Figure 13).

Predicted (Electrical Resistance Model –ERM) and measured resistance for hardening cement

Using the parameters K and the resistivity-time relationship (Fig. 13), the changes in the cement sheath resistance in the small model was predicted using the relationship in Eqn. (1). Figures 14 through Figure 19 show the variations of the predicted resistance value and also the actual measured values for different wire setup/combinations.

Vertical resistance

Wire setup-a

For the wire setup-a, the wire combination a1-a2 showed that the predicted values were lower than the measured values up to 14 days of curing but after that the measured resistance values were in the range of the predicted resistance (Figure 14). This may be because in the small model#2 the cement is hydrating under pressure and temperature and the resistivity used (Fig. 13) to predict the resistance was cured under room condition under no pressure.
For wire setup-a wire combination a1 and a4, the measured values were very close to the predicted values (Figure 15). The wire at level a4 is very close to the surface of the small model which showed very similar hydration to the test sample (Fig. 13). The measure resistance values matched very well with the predicted values.

Wire setup-b

For wire setup-b, the wire combination b1 and b3 showed that the predicted values were lower for about 30 days of curing (Figure 16). As mentioned before the initial hydration of small model was different from the samples curing in the 2-inch x 4-inch mold under room condition. After 1 month, the measured values matched very well with the predicted values since the curing temperatures were very similar.

For wire combination b1 and b4, the measured values are very close to the predicted values (Figure 17). Similar trend was observed with wire a1 and a4 (Fig. 15).

Wire setup-c

For wire setup-c, for the wire combination c1 and c2, the initial predicted values were slightly lower than the measured resistance as observed with setup-a and setup-b. In this region the cement was curing at a higher temperature and pressure as mentioned before. After two weeks of curing, the measured resistance matched very well with the predicted resistance (Fig. 18). And for wire combination c1 and c4, the measured values are within the range of the predicted values (Figure 19) which was similar to what was observed with setup-a and setup-b.

Pressure Test

Air pressure (P_i) was applied inside the casing to load the cement-sheath and the electrical resistance (R_o in Ohms) was measured between Level 1-2, Level 2-3, Level 3-4, Level 4-5 (Figure 5), were monitored while the air pressure was applied inside the casing (Figure 20).

Case 1: Initial Condition (No pressure, Pi = 0)

The variation of initial resistance is shown in Figure 21. The initial resistance was higher at the bottom (level 1-2) due to weight of the cement sheath and was lower at the top level (level 4-5). The electrical resistance increased with the depth and varied from 400 to 800 ohms (Fig. 21). This is partly due to the piezoresistive property of the smart cement, where the electrical resistance will be higher with increase in pressure with depth.

Case 2: Pi = 60 psi

Internal pressure of 60 psi was applied and the resistance changes were measured after 26 hours. The change in resistance was normalized with initial resistance $\Delta R/R(\%)$ is shown in Figure 22. The resistivity change in the smart cement due to the applied pressure was about 0.5 to 0.6%, indicating the piezoresistivity of the smart cement.

Case 3: Pi = 100 psi

Pressure of 100 psi was applied and the resistance changes were measured in 26 hours and reported in the form of $\Delta R/R$ (%) in Figure 22. The resistivity change in the smart cement due to the applied pressure of 100 psi was about 2.5%, indicating the piezoresistivity of the smart cement.

Case 3: Pi = 140 psi

Internal pressure of 140 psi was applied and the resistance changes were measured in 26 hours and reported in the form of $\Delta R/R$ in Fig. 22. The resistivity change in the smart cement due to the applied pressure was about 6.5 to 7%, indicating the piezoresitivity of the smart cement.

Piezoresistive Modeling

The stress at every point can be separated into mean stress and deviatoric stress. The change in the deviatoric stress due to the applied pressure (Pi) along the axis of the casing (z-axis) is represented as ΔS_{zz}. Using equilibrium and stress analyses, it can be shown that ΔS_{zz} is directly proportional to the applied internal pressure Pi. Hence the change in deviatoric stress can be represented as follows:

$$\Delta S_{zz} = f(Pi) \quad \ldots\ldots\ldots\ldots\ldots \quad (5)$$

The variation of internal applied pressure with the resistivity of smart cement (ρ_z) is shown in Fig. 23, and the response of the smart cement is nonlinear.

p, q model

The nonlinear p-q model was developed by Vipulanandan et al. (1990) and was used to predict $\Delta\rho_z/\rho_z$ variation with the applied pressure. The relationship can be represented as follows:

$$P_i = \frac{(\frac{\Delta\rho_z}{\rho_z})}{q+(1-q-p)(\frac{\Delta\rho_z}{\rho_z})+p(\frac{\Delta\rho_z}{\rho_z})^{\frac{p+q}{p}}} \quad \text{.....(6)}$$

The model parameters p and q were 1.2 and 3 respectively. Hence measuring the change resistivity of the smart cement it will be possible to predict the pressure in the casing and also the stress in the cement sheath.

Conclusions

Based on the resistivity monitoring and model study following conclusions are advanced.

(1) Two probe method was effective in measuring the bulk resistance of the drilling mud, spacer fluid and smart cement slurry. Based on the changes in resistance measurements it will be possible to identify the fluid rise in the well borehole.

(2) Using the laboratory model it was possible to demonstrate the real-time monitoring of the well bore with drilling mud, space fluid and smart cement slurry

(3) Using the concept developed in this study, it is possible to use the K parameter and predict the changes in the resistance of drilling and hardening smart cement.

(4) Using a nonlinear model the change in electrical resistivity of smart cement was related to the applied pressure in the casing. The smart cement was very sensitive to the applied pressure

References

1. API Recommended Practice 10B (1997), Recommended Practice for Testing Well Cements Exploration and Production Department, 22nd Edition.
2. API recommended Practice 65 (2002) Cementing Shallow Water Flow Zones in Deepwater Wells.
3. Carter, K. M. and Oort, E. (2014), Improved Regulatory Oversight Using Real- Time Data Monitoring Technologies in the Wake of Mocondo, SPE 170323, pp. 1-51.
4. Dom, P. B., S. Rabke, et al. (2007). "Development, verification, and improvement of a sediment-toxicity test for regulatory compliance." SPE Drilling & Completion, Vol. 22(2), 90-97.
5. Griffith, J. and Faul, R. (1997) "Mud Management Special Slurries Improve Deepwater Cementing Operations," Oil and Gas Journal, Vol. 95, No. 42, pp. 49-51.
6. Izon, D. and M. Mayes, M. (2007) "Absence of fatalities in blowouts encouraging in MMS study of OCS incidents 1992-2006," Well Control Magazine, pp. 86-90.
7. John B., (1992). "Class G and H Basic Oil Well Cements," World Cement.
8. Kim, J and Vipulanandan, C. (2006)"Removal of Lead from Contaminated Water and Clay Soil Using a Biosurfactant," Journal of Environmental Engineering, Vol. 132, No. 7, pp.857-865.
9. Kim, J. and Vipulanandan, C. (2003) "Effect of pH, Sulfate and Sodium on the EDTA titration of Calcium," Cement and Concrete Research, Vol. 33(5), pp. 621-627.
10. Kyle, M. and Van Eric (2014), Improved regulatory oversight using real- time data monitoring technologies in the Wake of Mocondo, SPE 170323, pp. 1-51.
11. Li, F., Vipulanandan, C. and Mohanty, K. (2003) "Microemulsion and Solution Approaches to Nanoparticle Iron Production for Degradation of Trichloroethylene," Colloids and Surfaces A: Physicochemical and Engineering Aspects, Vol. 223, No. 1, pp. 103-112.
12. Labibzadeh, M., Zhhabizadeh, B. and Khajehdezfuly, A., (2010) "Early Age Compressive Strength Assessment of Oil Well Class G Cement Due to Borehole Pressure and Temperature Changes, Journal of American Science, Vol. 6, No.7, pp.38-47.
13. Nam, M. S. and Vipulanandan, C. (2008) "Roughness and Unit Side Resistances of Drilled Shafts Socketed in Clay Shale and Limestone, Journal of Geotechnical and Geoenvironmental Engineering, Vol. 134, No. 9 , pp. 1272-1279.
14. Miranda C.R., Carvalho K.T., Vargas A.A., Rodrigues L.F., Marchesini F.H. (2007). "Minimizing fluid contamination during oil well cementing operations"; OMC 2007
15. Mirza, J. et al. (2002) "Basic Rheological and mechanical properties of High Volume Fly Ash Grouts," Construction and Building Materials, Vol. 16, pp.353-363.
16. Ozgurel, G., Gonzalez, H. A. and Vipulanandan, C., (2005) "Two dimensional Model Study on Infiltration Control at a Lateral Pipe Joint using Acrylamide Grout", Proceedings, Pipelines 2005, ASCE, pp. 631-642.
17. Park, J., Vipulanandan, C., Kim, J. and Oh, M. H. (2006) "Effect of Surfactants and Electrolyte Solutions on the Properties of Soils," Journal of Environmental Geology, Vol. 49, pp.977-989.
18. Ravi, K. et al. (2007) "Comparative Study of mechanical Properties of Density-reduced Cement Compositions, SPE Drilling & Completion, Vol. 22, No. 2, pp. 119-126.
19. Ramachandran, V. S. (1984) Concrete Admixture Handbook, Noyes Publication, Park Ridge, New Jersey, 628 pp.
20. Samsuri A., Junin R., Osman A.M. (2001). The utilization of Malaysian local bentonite as an extender and free water controller in oil-well cement technology, Society of Petroleum Engineers. Doi: 10.2118/68674-MS.
21. Sarap G.D., Sivanandan M., Patil S., Deshpande A.P. (2009) The use of high performance spacers for zonal isolation in high temperature High-pressure wells SPE/IADC 124275.

22. Thaemlitz, J., A. D. Patel, et al. (1999). "New environmentally safe high-temperature water-based drilling-fluid system." SPE Drilling & Completion Vol. 14(3), 185-189.
23. Vipulanandan, C. and Leung, M., (1991)" Seepage Control in Contaminated and Permeable Houston Clay: Laboratory Study," Hazardous Waste & Hazardous Materials, Vol. 8, No. 1, 17-32.
24. Vipulanandan, C. and Neelam Kumar, M.(2000) "Properties of Fly Ash-Cement Cellular Grouts for Sliplining and Backfilling Applications," Proceedings, Advances in Grouting and Ground Modification, ASCE, GSP 104, Denver, CO, pp. 200-214.
25. Vipulanandan, C., and Sett, K. (2004) "Development and Characterization of Piezoresistive Smart Structural Materials", Proceedings, Engineering, Construction and Operations in Challenging Environments, Earth & Space 2004, ASCE Aerospace Division, League City, TX, pp. 656-663.
26. Vipulanandan, C., and Liu, J. (2005) "Polyuretane Based Grouts for Deep Off-Shore Pipe-in-Pipe Application", Proceedings, Pipelines 2005, ASCE, Houston, TX, pp. 216-227.
27. Vipulanandan, C., and Garas, V. (2006), "Piezoresistivity of Carbon Fiber Reinforced Cement Mortar", Proceedings, Engineering, Construction and Operations in Challenging Environments, Earth & Space 2006, Proceedings ASCE Aerospace Division, League City, TX, CD-ROM.
28. Vipulanandan, C. and Mamidi, B. (2008**),"**Biosurfactant Flushing of PCE Contaminated Clayey Soils," Proceedings, GeoCongress 2008, Geotechnics of Waste Management and Remediation, ASCE, GSP 177, pp. 495-502.
29. Vipulanandan, C. and Nam, E. (2009), "Drilled Shaft Socketed in Uncemented Clay Shale," Proceedings, Foundation Congress 2009, Contemporary Topics in Deep Foundations, ASCE, GSP 185, pp. 151-158.
30. Vipulanandan, C. and Usluogullari, O. (2009), "Field Evaluation of A New Down-Hole Penetrometer" Proceedings, Contemporary Topics in In Situ Testing, Analysis, and Reliability of Foundations, Foundation Congress 2009, ASCE, GSP 186, pp. 119-126.
31. Vipulanandan, C., Dimrican, E. and Harendra, S. (2010) "Artificial Neural Network and Nonlinear Models for Gelling and Maximum Curing Temperature Rise in Polymer Grouts," Journal of Materials in Civil Engineering, Volume 23, No. 4, p. 1-6.
32. Vipulanandan, C. and Prasanth, P., (2013)" Impedance Spectroscopy Characterization of a piezoresistive Structural Polymer Composite Bulk Sensor," Journal of Testing and Evaluation, Vol. 41, No.6, 898-904.
33. Vipulanandan et al. (2014) "Development and Characterization of Smart Cement for Real Time Monitoring of Ultra-Deepwater Oil Well Cementing Applications, OTC-25099-MS.
34. Vipulanandan et al. (2014) "Characterization of Smart Cement Modified with Sodium Meta Silicate for Ultra-Deepwater Oil Well Cementing Applications, AADE-2014.
35. Vipulanandan, C. Heidari, M., Qu, Q., Farzam, H., and Pappas, J. M. (2014), "Behaviour of piezoresistive smart cement contaminated with oil based drilling mud," Offshore Technology Conference, OTC 25200-MS, pp. 1-14.
36. C. Vipulanandan, C. and A. Mohammed, A. (2014), "Hyperbolic rheological model with shear stress limit for acrylamide polymer modified bentonite drilling muds," Journal of Petroleum Science and Engineering, 122 (2014) 38–47.
37. Wang, S. Y. and Vipulanandan, C., (1996) "Leachability of Lead From Solidified Cement-Fly Ash Binders," Cement and Concrete Research, Vol. 26, No. 6, pp. 895-905.
38. Zhang M., Sisomphon K., Ng T.S, and Sun D.J, (2010). "Effect of superplasticizers on workability retention and initial setting time of cement pastes," Construction and Building Materials 24, 1700–1707.
39. Zhang J., Weissinger E.A, Peethamparan S, and Scherer G.W., (2010). "Early hydration and setting of oil well cement," Cement and Concrete research, Vol. 40, 1023-1033.

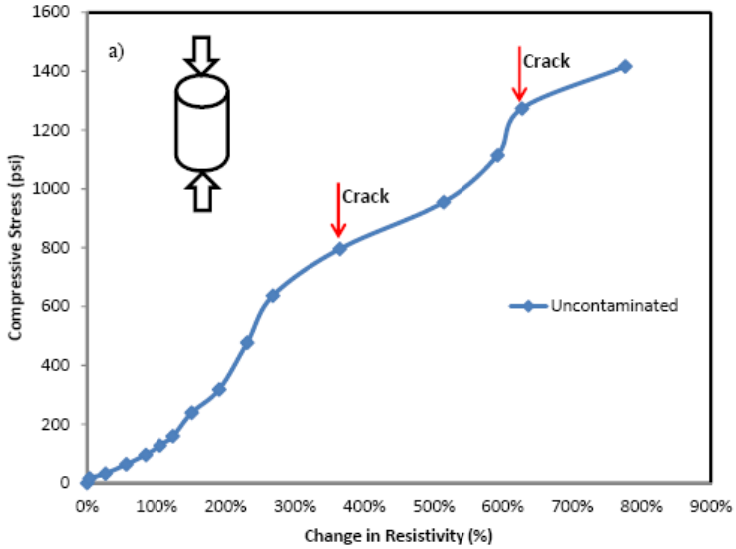

Figure 4. Typical Piezoresistivity Behavior of Oil Well Cement with 0.075% CF after one day of curing (AC frequency =300 kHz)

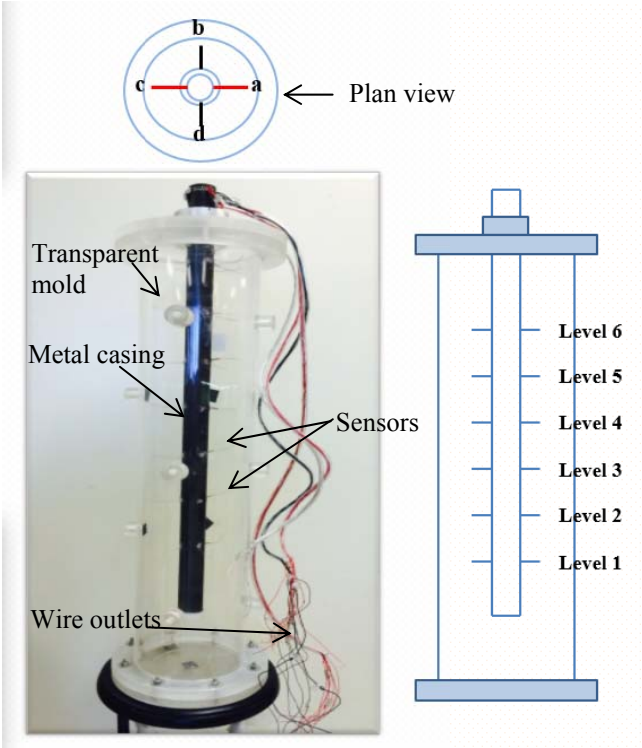

(a) Lab model

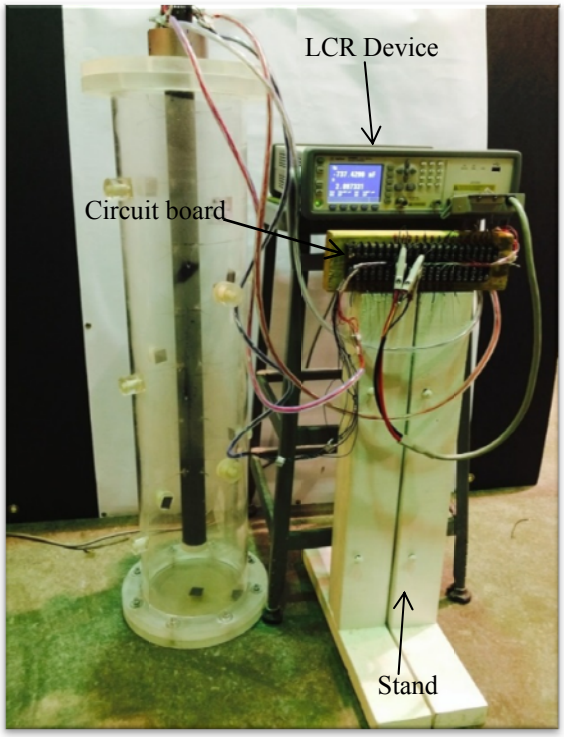

(b) Monitoring System

Figure 5. Laboratory scale oil well model and monitoring system

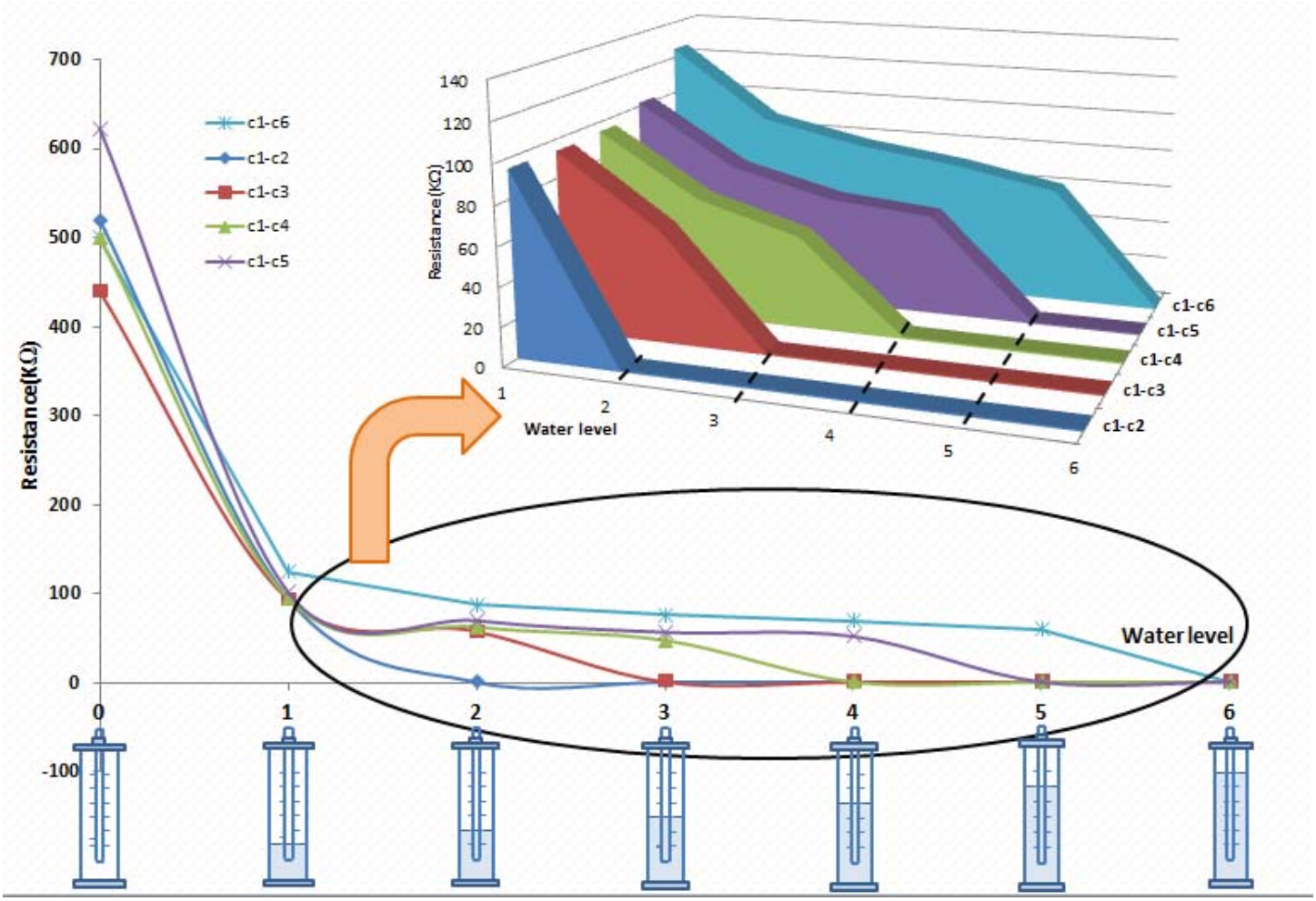

Figure 6. Vertical resistance measurement in the oil small model with changing water level

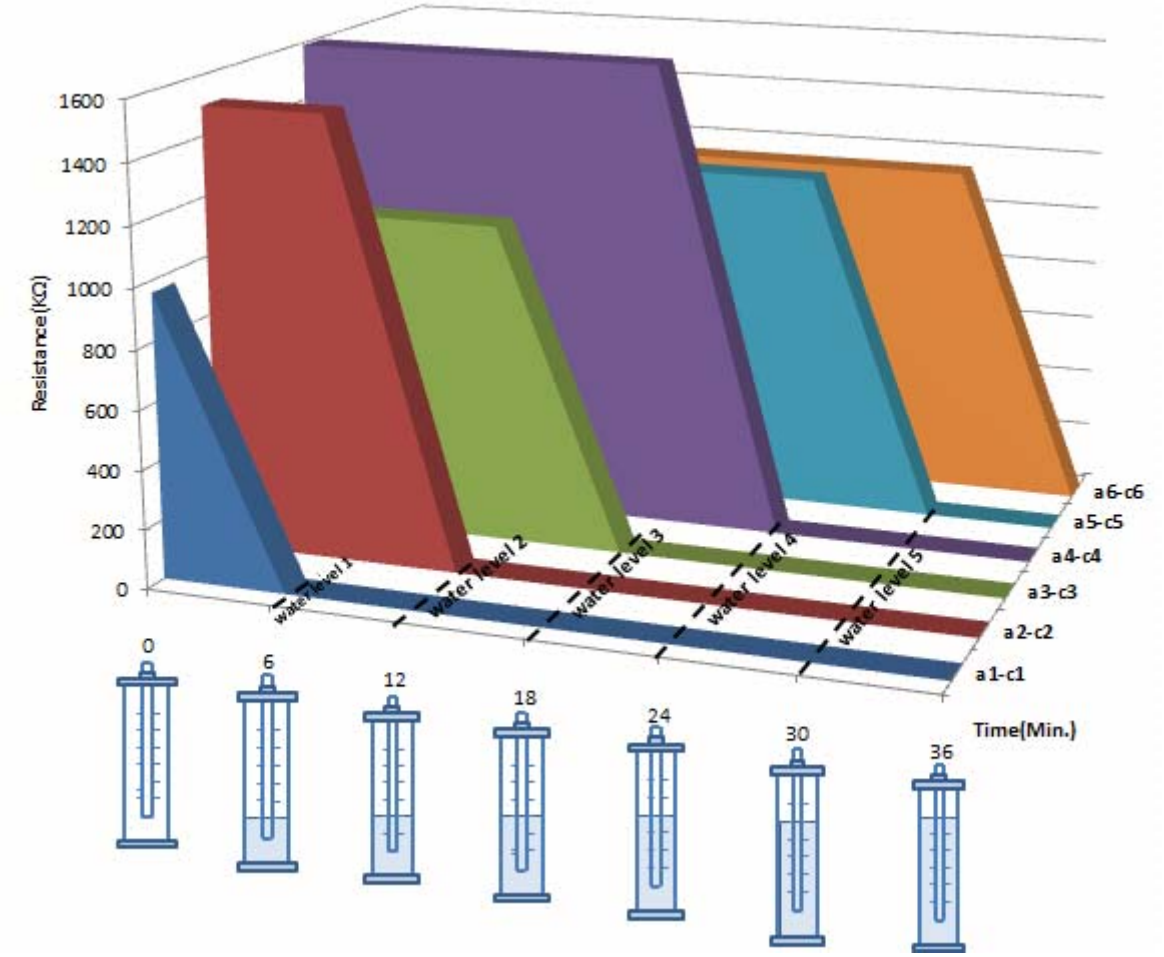

Figure 7. Horizontal resistance measurements with varying heights of water level

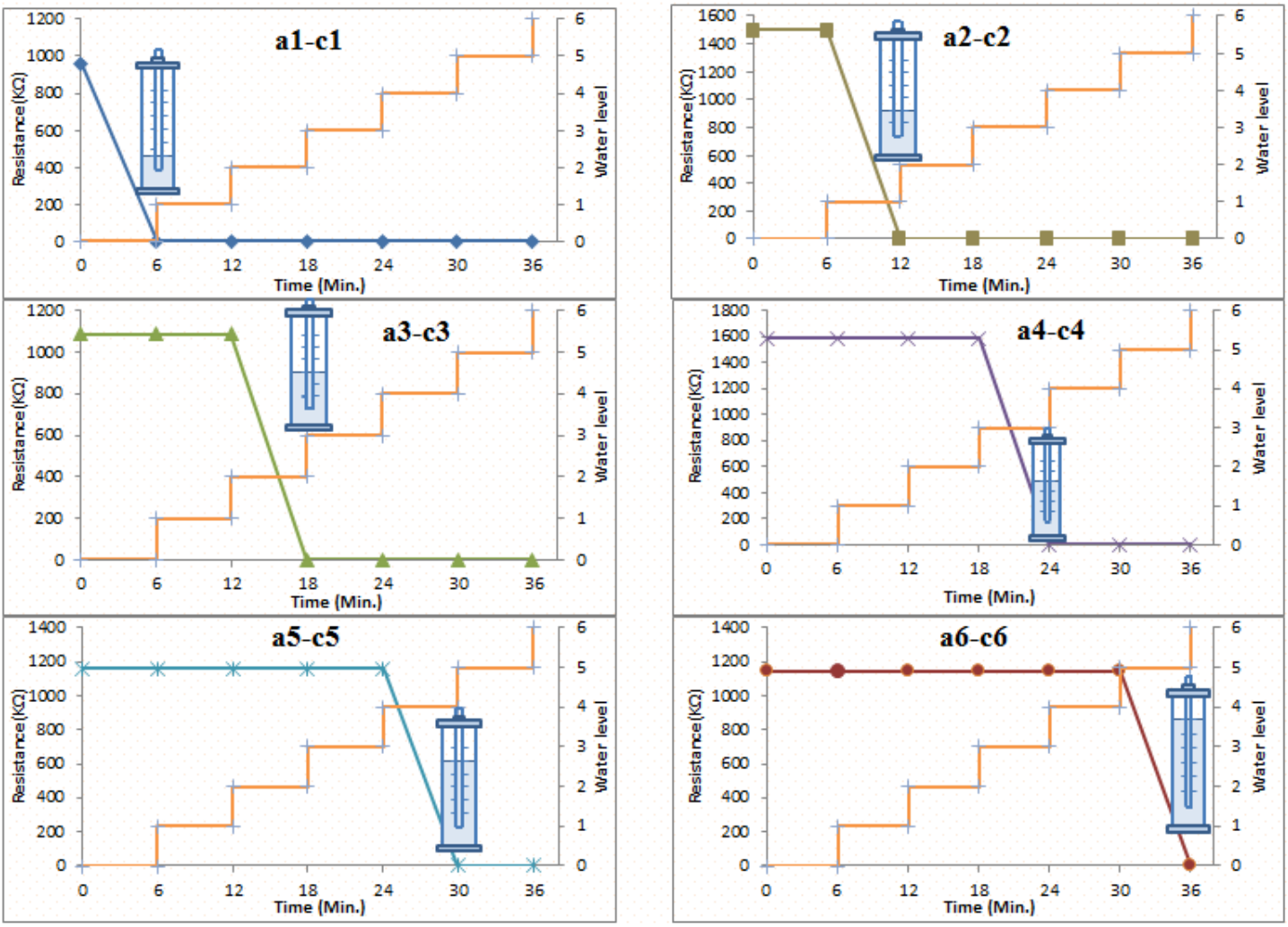

Figure 8. Variation of resistance with rising water level

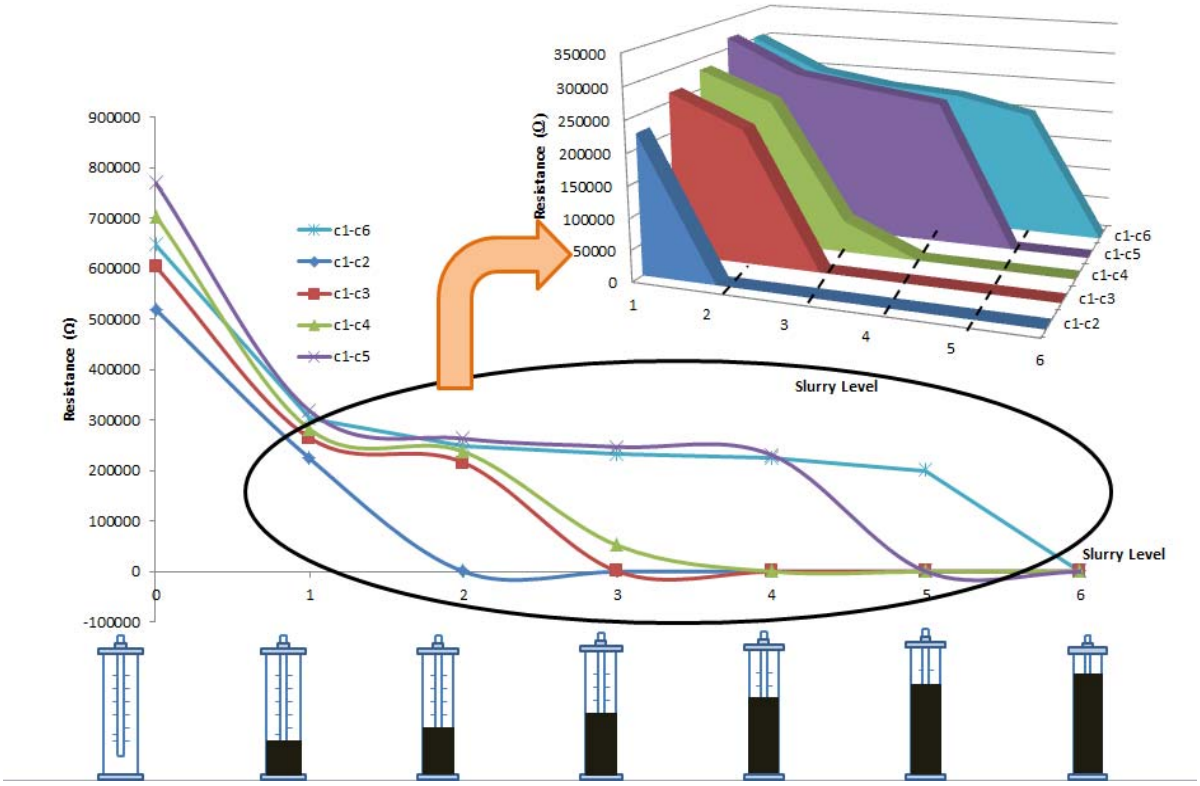

Figure 9. Variation of vertical resistance with different level of cement slurry

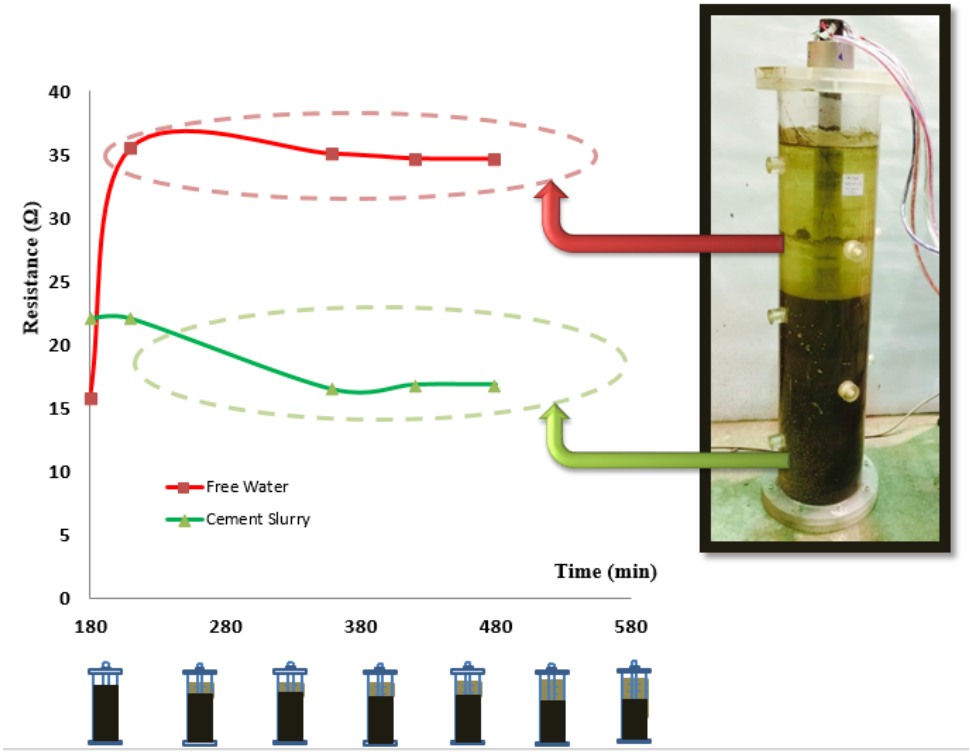

Figure 10. Resistance for free water and cement slurry

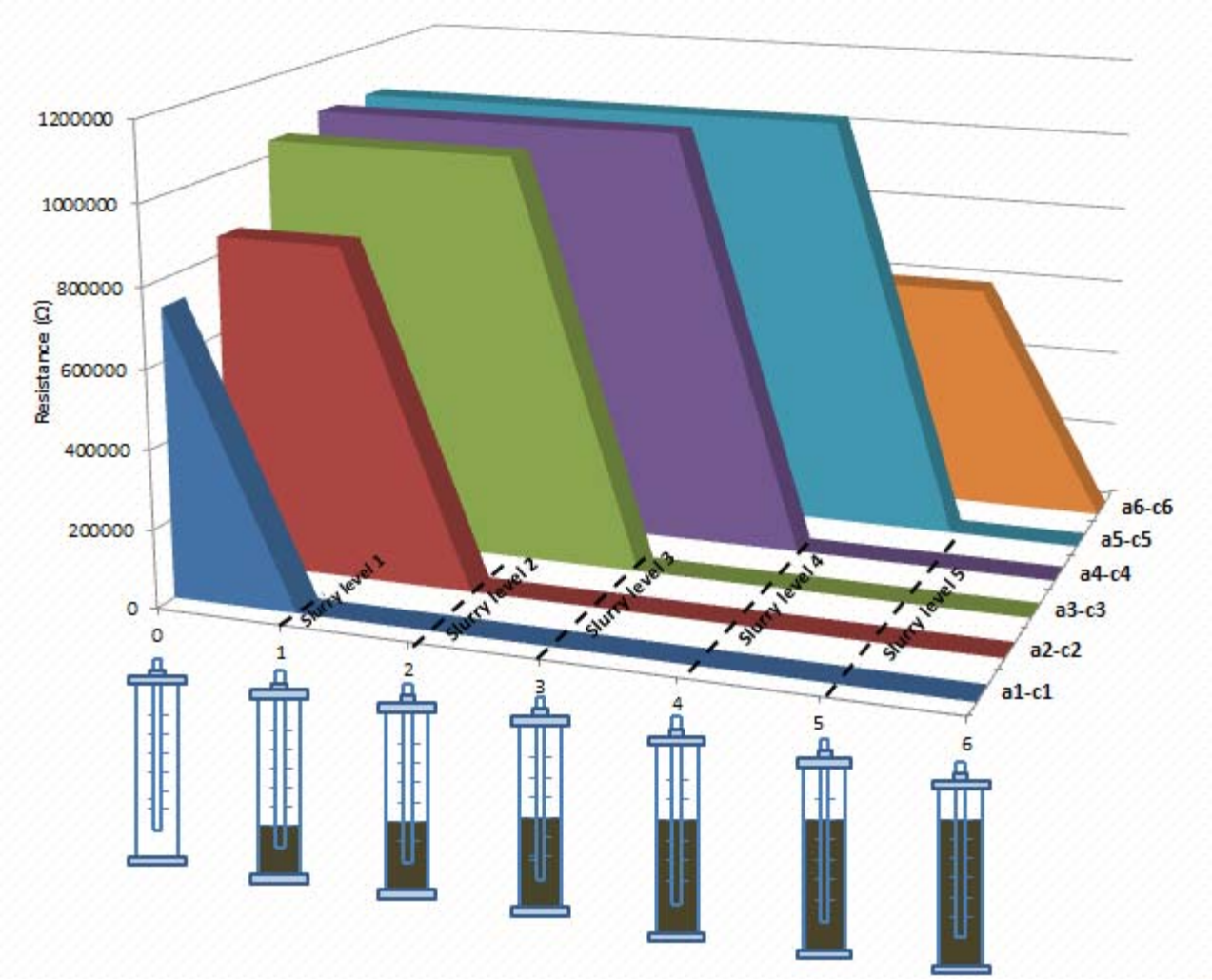

Figure 11. Horizontal slurry resistance with slurry level

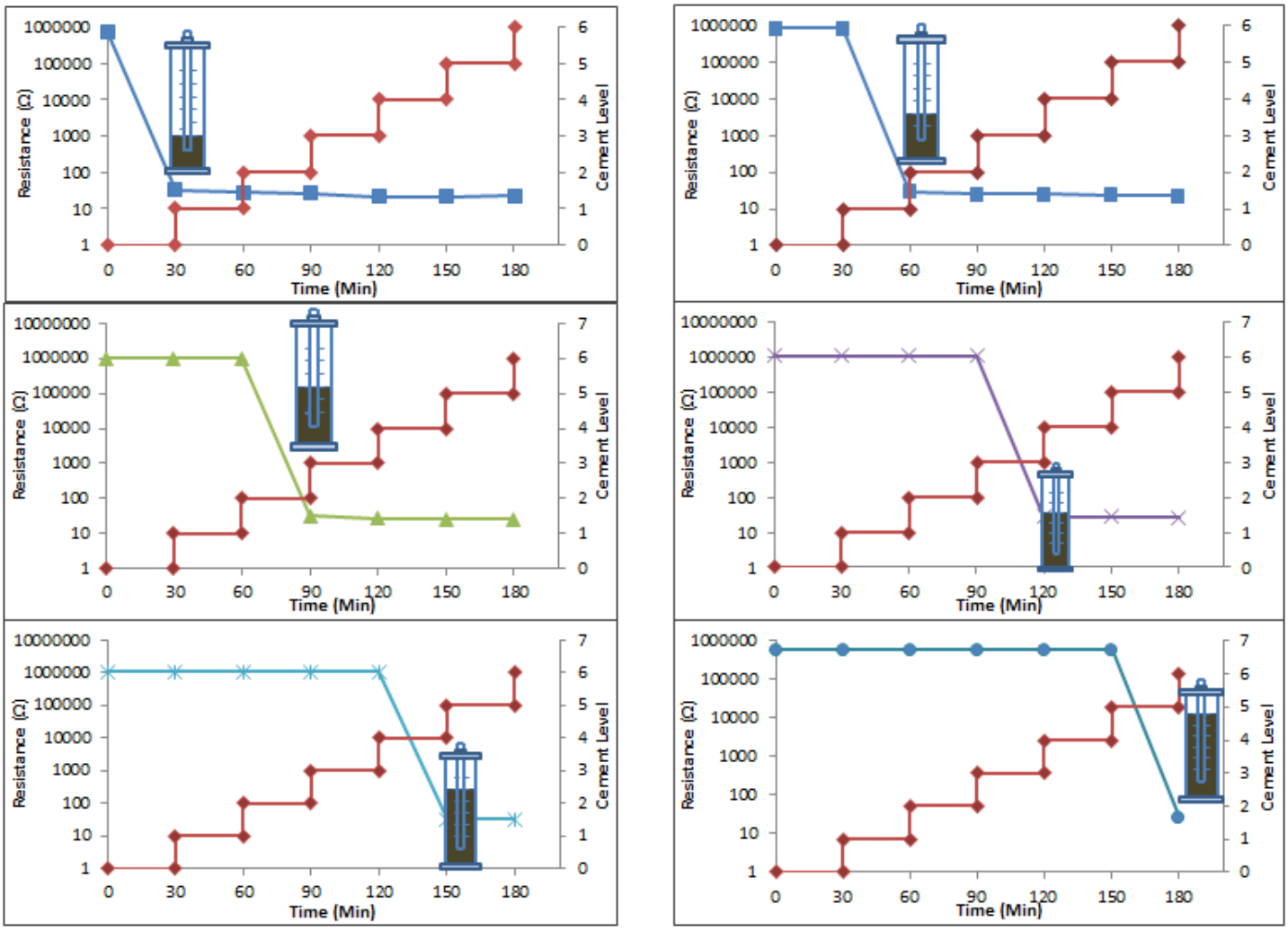

Figure 12. Horizontal resistance variation of cement slurry with slurry level

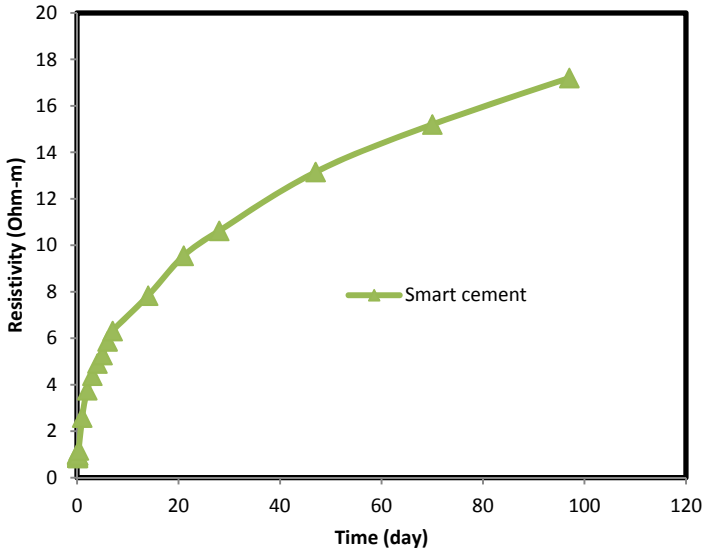

Figure 13. Variation of smart cement resistivity with curing time for samples cured under room conditions (23°C and 50% relative humidity (RH))

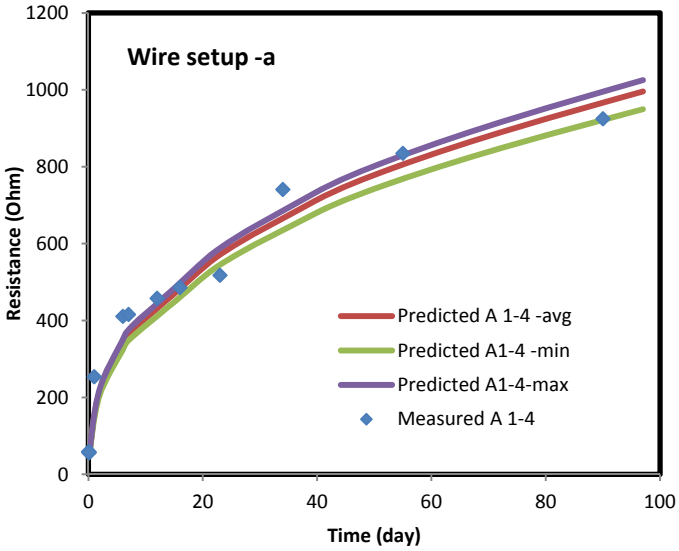

Figure 15. Predicted and measured resistance for wire setup A for wire combination a1-a4

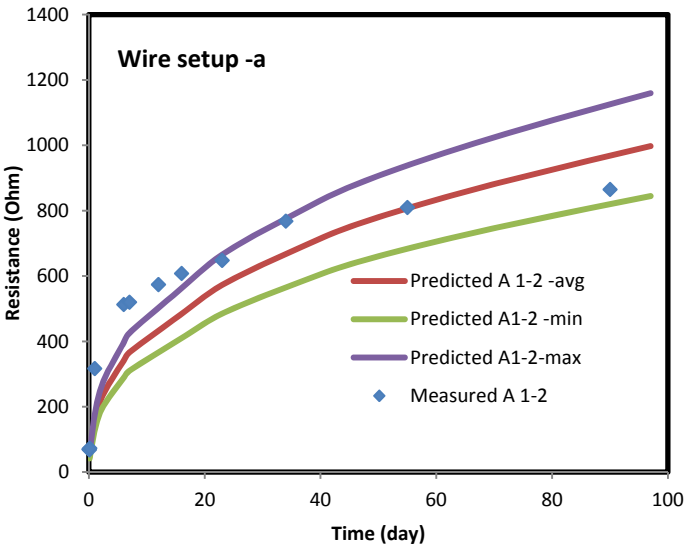

Figure 14. Comparing the predicted and measured resistance for wire setup-a for wire combination a1-a2.

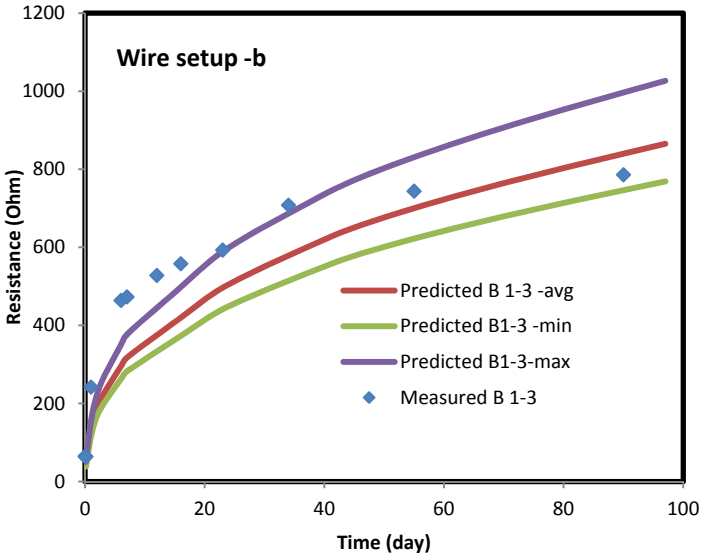

Figure 16. Predicted and measured resistance for wire setup B for wire combination b1 and b3

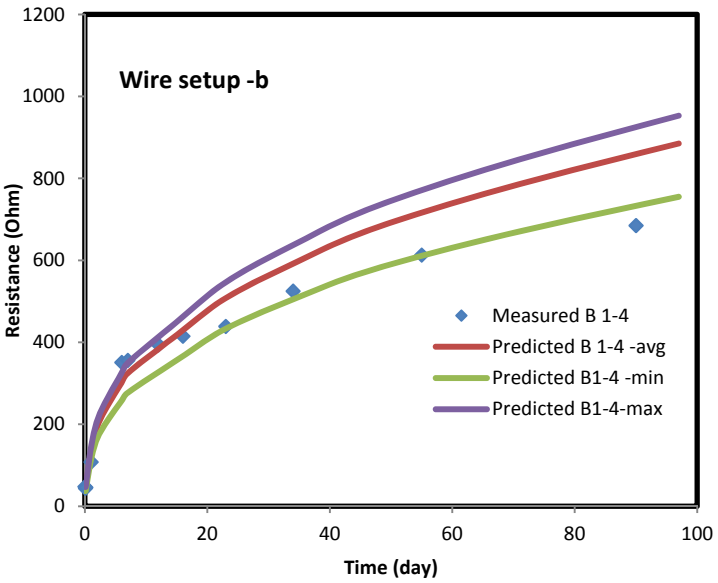

Figure 17. Predicted and measured resistance for wire setup B for wire combination b1 and b4.

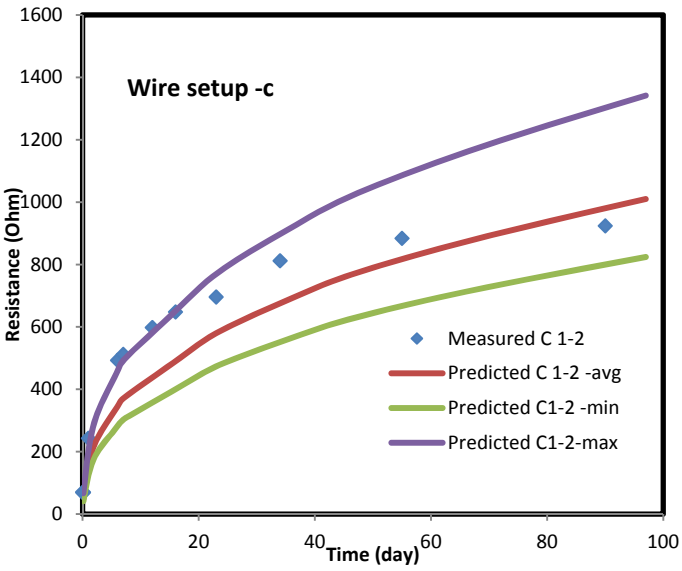

Figure 18. Predicted and measured resistance for wire setup C for wire combination c1 and c2.

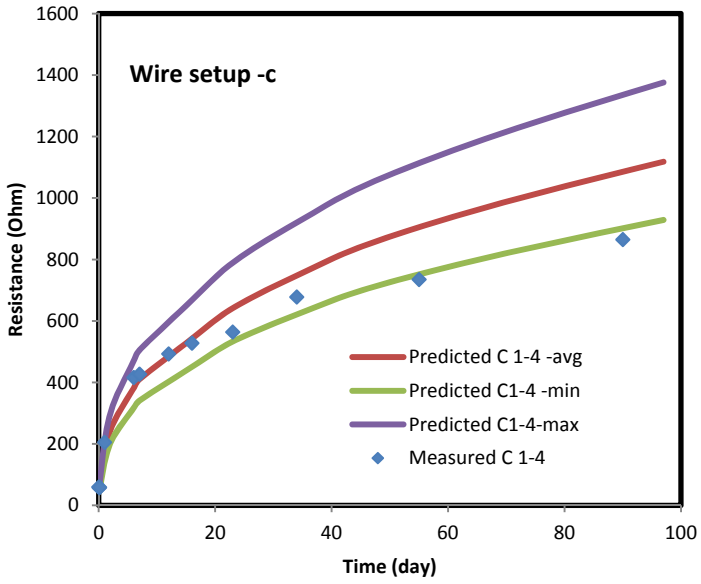

Figure 19. Predicted and measured resistance for wire setup C for wire combination c1 and c4.

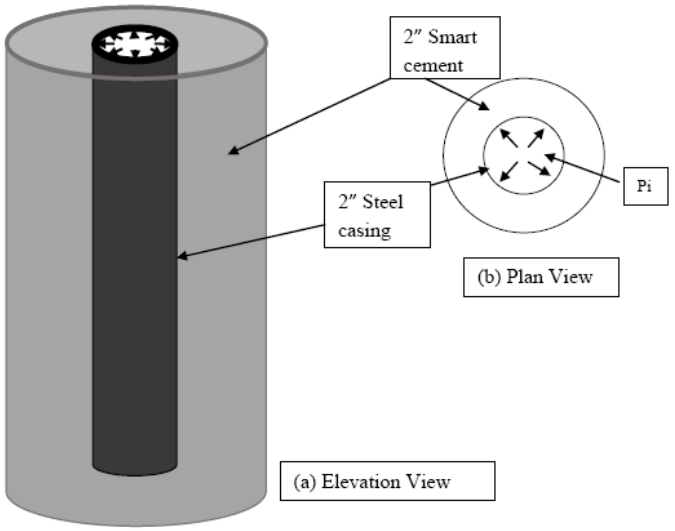

Figure 20. The configuration of the pressure applied in the inside the steel casing

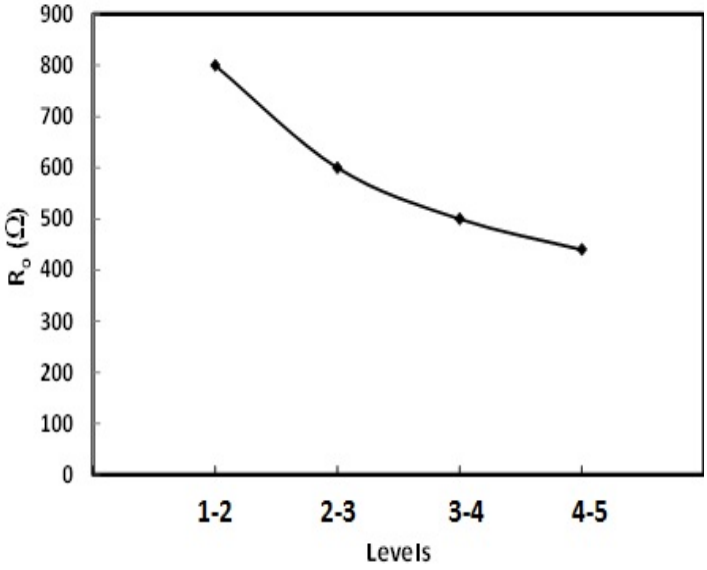

Figure 21. Variation of initial resistance with depth after 100 days of curing

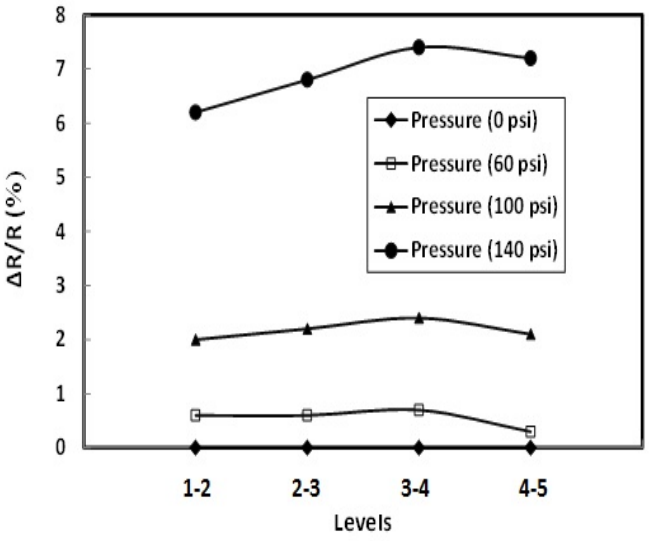

Figure 22. The changes in resistance with applied pressure for smart cement after 100 days of curing

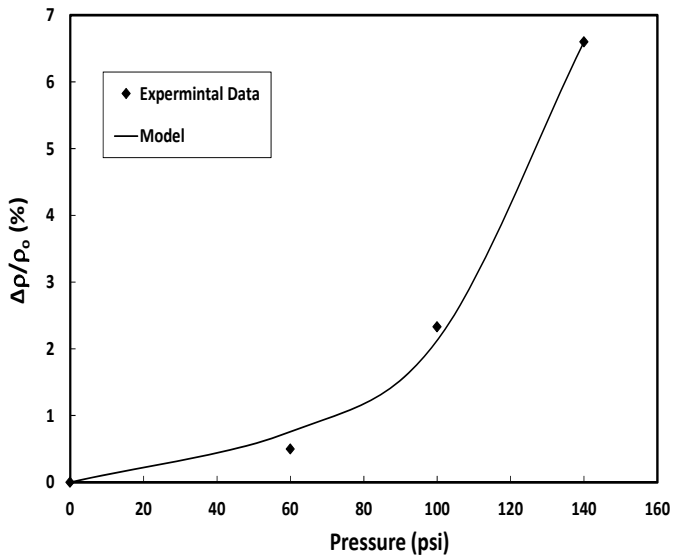

Figure 23. Model prediction of changes in resistivity with applied pressure for smart cement after 100 days of curing.